https://doi.org/10.5194/egusphere-2026-4932
Preprint. Discussion started: 10 September 2026

A Chamber-Based Experimental Framework for Comprehensive Mechanistic Studies of Ageing-Driven Changes in Biomass-Burning Aerosol Properties

Sara Aisyah Syafira[1,a], Aristeidis Voliotis[1,2], Dawei Hu[1], Osayomwanbor Oghama[1], Huihui Wu[1,2,b], Yunqi Shao[1], Rhianna Evans[3,c], Jie Chen[4], Yu Wang[5], Peter Gallimore[1,2], James Allan[1,2], Hugh Coe[1], Gordon McFiggans[1]

[1]Centre for Atmospheric Science, Department of Earth and Environmental Sciences, School of Natural Sciences, University of Manchester, Manchester, M13 9PL, UK
[2]National Centre for Atmospheric Science (NCAS), University of Manchester, Manchester, M13 9PL, UK
[3]Wolfson Atmospheric Chemistry Laboratories, Department of Chemistry, University of York, York, YO105DD, UK
[4]Institute for Atmospheric and Climate Science, Universitätstrasse 16, 8092 Zürich, Switzerland
[5]School of Geosciences, University of Edinburgh, College of Science and Engineering, EH9 3JW, United Kingdom
[a]Now at: Research Centre for Climate and Atmosphere (PRIMA), National Research and Innovation Agency (BRIN), Indonesia
[b]Now at: Université Paris Cité and Univ Paris Est Créteil, CNRS, LISA, F-75013 Paris, France
[c]Now at: Department of Environmental Toxicology, University of California, Davis, Davis, California 95616, USA.

Correspondence to: Aristeidis Voliotis (aristeidis.voliotis@manchester.ac.uk) and Gordon McFiggans (g.mcfiggans@manchester.ac.uk)

Abstract. Biomass burning (BB) aerosol particles can significantly impact climate, air quality, and human health. While studies have advanced our understanding of the impact-related properties of the particles, detailed investigations of both driving factors and mechanisms under controlled conditions of dark aging or photooxidation remain limited, especially across fuel types and burn phases. Here, we describe a BB aerosol facility at the University of Manchester that couples an Esse 175F commercial wood-burning stove, housed in a mobile unit outside the main laboratory and supplied with ambient combustion air, to the 18 m³ Manchester Aerosol Chamber. The facility enables batch-mode experiments under controlled dilution, temperature, relative humidity, oxidant exposure, target initial particle mass loading, and dark or illuminated aging conditions. Its batch configuration uses moderate, rather than high, continuous dilution, thereby limiting rapid dilution-induced perturbations while maintaining stable conditions and particle concentrations suitable for filter-based analyses, long-term parallel continuous measurements, and slow-response instruments that are difficult to deploy in short-residence-time flow systems. Measurements include particle size distribution, chemical composition, black carbon, volatility, hygroscopic growth, cloud condensation nuclei activity, optical properties, ice-nucleating ability, and gases. This facility, therefore, provides a repeatable, flexible system and platform for mechanistic and multiparameter investigation of fresh and aged BB aerosol. Experiments conducted in April and September 2022 demonstrated those capabilities across fuel types and combustion phases. They also characterized the facility, showing low background PM levels (<1 μg/m³), with primary gases and PM concentrations typically stabilizing within no more than 10–30 minutes after smoke injection.

https://doi.org/10.5194/egusphere-2026-4932
Preprint. Discussion started: 10 September 2026

1 Introduction

Recent large-scale fire events, such as those in British Columbia (Canada, 2017) and during Australia's "Black Summer" (2019–2020), have highlighted the growing frequency and severity of wildfires worldwide (Solomon et al., 2022; Stockwell et al., 2022). The resulting smokes of that biomass burning (BB) play a significant role in atmospheric pollution and climate forcing, contributing both primary particulate matter (PM) and precursor gases for secondary particulate (PM) formation (Hodshire et al., 2019; Hatch et al., 2017, Cobin et al., 2014; Grieshop et al., 2009). The implications span all scales—from local air quality and visibility to regional public health and global climate change (Chen et al., 2016; Iraci et al., 2022). Those impacts are governed not only by total particle concentrations but also by interacting physicochemical properties (Ching et al 2019). Particle size, chemical composition, morphology, and mixing state influence light scattering and absorption, hygroscopic growth, cloud condensation nuclei activity, ice-nucleating ability, atmospheric lifetime, and respiratory deposition (Ching et al., 2019; Zhai et al., 2017; Cobin et al., 2014). These properties continue to evolve upon dilution, transport, and aging.

While extensive ground-based, aircraft, and satellite observations have provided critical insights into the spatial and temporal extent of open biomass burning (Stockwell CE et al., 2022; Zhong Q et al., 2022; Patoulias D et al., 2021; Zhuravleva TB et al., 2021), they remain limited in their ability to resolve the detailed physicochemical evolution of emissions. The complexity of real-world fires (Hoi K-C et al 2013; Tang R et al 2020; Marsavin A et al 2023; Hodshire AL et al, 2019)—including variations in combustion conditions, fuel composition, moisture content (Price-Allison et al., 2019, 2023), and meteorology—hinders accurate mechanistic understanding of pollutant formation, transformation, and atmospheric aging. To overcome these challenges, laboratory-based simulations in controlled environments are crucial.

Chamber studies reduce many atmospheric uncertainties and allow repeatable experiments across a wide range of parameters. However, existing studies often target specific fuel types (e.g., wood), leaving emissions from other materials (e.g., leaves, peat, agricultural waste) less characterized (Roson et al., 2021; Yao et al., 2023). Additionally, experimental designs and methodologies often vary, making intercomparison between facilities and datasets difficult. Comparisons across facilities are further complicated by differences in aging protocols, dilution practices, and fuel-handling procedures, which has motivated the recent introduction of a standardized three-layer framework for cross-facility comparisons of biomass-burning aerosol studies (Syafira et al. 2026). While several chamber infrastructures have been developed to study biomass burning emissions—such as FLAME (Stockwell et al., 2015; McMeeking et al., 2009; Levin et al., 2010; Hennigan et al., 2011; Engelhart et al., 2012; Ortega et al., 2013), PSI (Bertrand et al., 2017), ILMARI-UEF (Tiitta et al., 2016; Leskinen et al., 2015), and CESAM (Wang et al., 2022)—most are optimized for specific biomass types, focus on short-duration processes, or rely on flow-through configurations that limit compatibility with slow-integration instruments.

To this end, a well-characterized, systematic, and flexible platform that supports batch-mode aging and multi-instrument compatibility, while being able to simulate real-world burning conditions across diverse fuel types and burn phases, is needed.

https://doi.org/10.5194/egusphere-2026-4932
Preprint. Discussion started: 10 September 2026

Additionally, combinations of comprehensive online and offline analytical techniques to examine properties and behaviour during simulated atmospheric processes provide a powerful tool to probe the atmospheric transformations, fate, and impacts of BB aerosol. The coupling of Manchester Aerosol Chamber (MAC) with a biomass burning capability described here is intended to achieve those gap aims, utilizing moderate dilution rather than high, continuous dilution to support long-term measurements by maintaining stable conditions and sufficient initial particle concentrations, with relatively non-excessive early dilution-driven chemical and physical changes.

The University of Manchester (UoM) biomass-burning facility, along with other facilities consisting of a coupled combustion source and a batch reactor connected by a subsampling system, fell into Category VIIa in the taxonomy of Syafira et al. (2026). However, this facility represents an unconventional configuration within Category VIIa, where the stove is located outside the laboratory and supplied with ambient air, providing more realistic combustion conditions than a closed system while retaining greater experimental control than open burning. The use of the stove in the current facility enables BB experiments using different biomass fuels and operationally selected burn phases. Specifically, the Esse 175F commercial wood stove used at UoM features a removable catalytic filter compartment for Ecodesign compliance, enabling experiments under either modern-appliance operation or conventional filter-free stove operation within a single device. This configuration distinguishes the facility from combustion in other combustion–chamber systems, such as the masonry heater at ILMARI (Tiitta et al., 2016), the residential wood stove at PSI (Bruns et al., 2015), or the open-burning fuel bed at FSL (Stockwell et al., 2014). On the other hand, comprehensive online measurement instruments were installed in the facility, including measurements of micron- and submicron-particle number concentrations, particle size distribution, chemical composition, black carbon, volatility, hygroscopic growth, cloud-condensation-nuclei activity, optical properties, and gases. Meanwhile, the attached integrated particle-filter samplings support detailed offline chemical composition analysis and assessment of ice-nucleation ability.

This current manuscript provides a full description and characterization of the biomass-burning facility built at the University of Manchester, along with its experimental framework and procedures, building on the separate characterization of its chamber (the Manchester Aerosol Chamber, MAC) in Shao et al. (2022). Results from measurements made during the April and September 2022 experimental campaigns are used here to characterize facility operation, assess background cleanliness and signal stabilization after smoke injection, and illustrate the facility's capability for multiparameter studies of fresh and aged biomass-burning aerosol, supporting future mechanistic studies of BB smoke important impacts-related properties and evolution.

2 Facility Description

2.1 Experimental Setup

The biomass burning (BB) aerosol study facility at University of Manchester couples the existing Manchester Aerosol Chamber (MAC, Shao et al. 2022) to a commercial Ecodesign-ready wood-burning stove (Esse 175F; https://www.esse.com/heating-

https://doi.org/10.5194/egusphere-2026-4932
Preprint. Discussion started: 10 September 2026

products/stoves/esse-175-f/) and a comprehensive suite of instrumentation. The catalytic filter compartment of the Esse 175F stove enabling the "Precision Burning" re-burn technology for Ecodesign compliance is removable, enabling a range of exhaust conditions to be explored (representing both modern abatement technologies as well as more conventional residential or wildfire conditions). Removing this filter and compartment results in a conventional stove configuration with air: fuel ratio (and hence burn condition) controlled by primary air restriction with secondary air from the back of the stove ensuring balanced draw and even air flow around the fuel bed.

Figure 1 illustrates the whole facility along with the installed instruments and the connecting lines. Fuel is burnt inside the stove located outside the laboratory building, using ambient unfiltered air. Exhaust is subsampled from a port in the 125mm diameter flue with controlled first-stage compressed air dilution delivered via a mass flow controller (MFC) to prevent water condensation on cooling. Diluted emissions are drawn into the MAC located on the ground floor of the laboratory building using a modified ejector diluter (Dekati® eDiluter™ Pro) installed in front of the MAC inlet port. A bespoke dilution bypass can be used to ensure the unit acts solely as an injector.

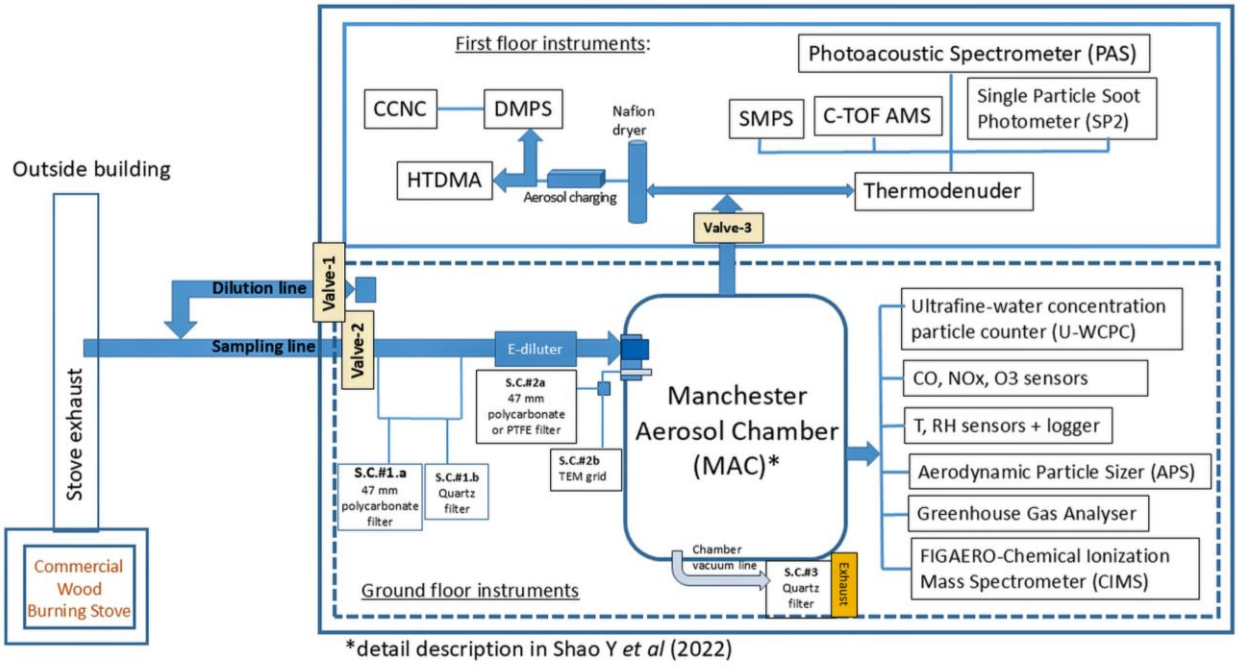

Figure 1: UoM Biomass Burning Aerosol Study Facility Scheme. **Note**: S.C. refers to sample collection

The Manchester Aerosol Chamber (MAC) is described in detail by Shao et al. (2022). Briefly, it is a batch reactor comprising a four-piece FEP Teflon bag sealed and suspended between a central fixed and two counter-weighted moving, rectangular extruded aluminium frames, forming a fully expanded volume of 18 m^3 (3 x 3 x 2 m). The bag is housed in an air-conditioned enclosure and optionally illuminated with two 6kW Xenon arc lamps and a bank of 7x16 halogen lamps. Laboratory air is fed at high flow

https://doi.org/10.5194/egusphere-2026-4932
Preprint. Discussion started: 10 September 2026

rate ($3m^3\ min^{-1}$) to the chamber through an air drier, followed by charcoal, Purafil, and HEPA filters, with an optional humidifier, ozone generator, and seed aerosol generator, and injection ports through a Teflon manifold block for conditioning gases and sources of sample air. Sample lines pass through manifold blocks such that all internal surfaces of the chamber are either Teflon or stainless steel. All flow valves and chamber components are adjustable and controllable from an automated interface with programmable cleaning, pre-experiment, and post-experiment cycles, with monitoring of all chamber parameters (including temperature and relative humidity). Before cleaning, at the end of each experiment, the entire remaining chamber contents are flushed through a filter in the main outlet.

The standard operating of the coupled facility follows this sequence

- fuel loading and ignition using kindling
- burn phase targeting: visual identification of flaming or smouldering for valve-2 control, as shown in **Fig.1**., for subsequent injection
- smoke dilution and injection into MAC
- fresh emission particle filter collection for offline analysis
- mixing period (~30 minutes)
- dark or photochemical aging using full-spectrum (UV plus visible) lamp exposure
- online sampling and offline filter collection

For detailed chamber design and instrumentation interfaces, refer to Shao et al. (2022).

2.1.1 MAC Operational Procedure in the Biomass Burning Experiments

Operation of the MAC during the experiments follows the standard procedures detailed in Shao et al. (2022), with minor modifications, such that the first stage diluted smoke is injected into the chamber during its last fill cycle. Four pre-experiment fill-flush cycles were sufficient to reduce particle number and mass concentrations to below 100 particles/cm3 and 1 ug/m3, respectively. The target RH setpoint during the burning experiments is typically 50-60%, though this can be manually adjusted to any nominal value below that of the injected first stage diluted smoke. The programmed pre-experiment procedure is stopped manually several minutes after the start of the last fill cycle such that the chamber is around 1/3 full prior to smoke injection. On each burning experiment day, the programmed pre-experiment and post-experiment procedures are routinely applied, with an additional “harsh cleaning” procedure conducted weekly

2.1.2 Stove Preparation and Fuel Burning

Ignition is initiated with kindling from the same wood stock as the primary fuel where possible (see below), with the stove door and ventilation open. One or more test pieces of the fuel are then added prior to closing the stove door, with the stove ventilation open. The influence of burn phase is investigated by sampling to the MAC during only the smouldering or flaming phase, visually

https://doi.org/10.5194/egusphere-2026-4932
Preprint. Discussion started: 10 September 2026

distinguishing them to direct the control of **valve-2**. For sampling of smouldering emissions, the stove ventilation is closed to reduce/limit the burning ambient air and smoke injection initiated only once flame was visually absent. Only smouldering phase combustion is possible for some less combustible fuels (e.g., peat, leaves). Small pieces of wood kindling are used for ignition with leaves and peat, with both the stove door and ventilation open, closing the door once ignition started. After complete consumption of the ignition materials and disappearance of any flame, smoke produced from leaves or peat (or similar low combustibility fuels) can be directly sampled.

2.1.3 Smoke sampling, dilution, and injection into the MAC

Smoke from the flue stack is sampled through a ½ inch (12.5 mm) diameter pipe connected to the e-diluter described in **Sect. 2.1.** First stage smoke dilution is conducted using dry compressed laboratory air delivered at 2 L/minute to the sampling line using a Y-splitter to prevent condensation in the sample line on cooling prior to the e-diluter. The e-diluter is used solely as an ejector following a modification that diverted the excess flow back into the chamber.

During smoke injection, the filling of the chamber bag with filtered dry air is continued intermittently to avoid overfilling and enabling humidity adjustment by altering the valve positions to the humidifier. Smoke injection is continued until the total particle mass concentration measured in the chamber reaches the target levels.

2.2 Fuel Types and Combustion Conditions

Four types of fuel were used to evaluate elements of the facility's performance under controlled laboratory conditions. Where possible, each fuel was combusted in either flaming or smouldering phase and emissions were aged under either dark or photochemical conditions**.** Each experiment included real-time PM and gas monitoring, along with optional offline sampling.

The fuels used for facility characterization were leaves (hornbeam), dry peat, kiln-dried hardwood (beech) and softwood (pine). The wood's moisture content was around 8-9% according to a digital moisture meter. Peat and the wood fuels were roughly similar sizes before being loaded into the stove. Fuel weight was not specifically controlled in this set of experiments but can be explored in the future for emission factor-type studies. A full list of the experiments used for characterization can be found in Table S1, Supplementary Information Section S1.

2.3 Instrumentation

A wide range of online and offline instruments can be deployed for particle and gas-phase emission measurements. Standard instrumentation (e.g., O_3, NO_x analyzers) was used to monitor photochemistry and gas evolution, with a range of others deployed on demand. Those used in the facility characterization experiments are listed in **Table 1**. Detailed specifications, calibration protocols, and operating specifics for each instrument are provided in Section 1 (S1.1), Supplementary Information.

https://doi.org/10.5194/egusphere-2026-4932
Preprint. Discussion started: 10 September 2026

Table 1. Available instrumentation

Instrument	Measurement	Purpose	Duty Cycle
AMS	Non-refractory PM composition	Organic/inorganic aerosol quantification	Continuous
SP2	Refractory black carbon	BC core mass and mixing state	Continuous
HTDMA	Size-resolved hygroscopic growth	Hygroscopicity (κ), growth factor	1-hour
CCNc	CCN activation curves	Cloud droplet activation (D_{50}, κ)	1-hour
CIMS	High-res gas-phase organics	VOCs, oxidation products	Continuous
SMPS/DMPS	Size-resolved number concentrations	Particle size distribution, volume	Continuous
PASS	Particle Optical Properties	Particle Optical Properties	Continuous

2.4 Filter Sampling and Offline Analysis

Three approaches have been used for filter sampling:

1. End-of-experiment total PM collection via a custom chamber-exhaust filter holder, capturing all particles post-aging. (Evans et al., 2025; Evans et al., 2024; Shao et al., 2022) at position **S.C.#3** in **Fig.1**.
2. Fresh first-stage diluted smoke inline sampling via a 47 mm polycarbonate filter or Quartz filter (Whatman QMA, 47 mm) at position **S.C.#1. a**. and position **S.C.#1. b.** in **Fig.1,** respectively (Chen et al., 2024; Evans et al., 2024).
3. Fresh and aged second-stage diluted (i.e., chamber diluted) smoke sampling using either a 47 mm polycarbonate filter (Chen et al., 2024) or a PTFE filter (Oghama et al., 2026; Oghama et al., 2025), and a TEM grid (Pella, Inc., 01754-F) (Chen et al., 2024), at position **S.C.#2. a**. and position **S.C.#2. b.** in **Fig.1,** respectively. (Chen et al., 2024; Evans et al., 2024).

Collected filters were analyzed using:

- UHPLC-Orbitrap MS for detailed organic compound profiling (Evans et al., 2025; Evans et al., 2024) of the filtered sample at position **S.C.#1. b.** and position **S.C.#3**
- FIGAERO-CIMS for thermochemical volatility and oxidation studies (Oghama et al 2026; Oghama et al 2025; Bannan et al., 2019; Voliotis et al., 2021)
- Droplet ice nuclei counter Zurich (DRINCZ) and microfluidics ice nuclei counter Zurich (MINCZ, Isenrichet al.24) for ice nucleation measurements of bulk BBA and chemical (Chen et al., 2024).
- Synchrotron-based scanning transmission X-ray microscopy (STXM) coupled with near-edge X-ray absorption fine structure spectroscopy (NEXAFS) for morphology analysis of individual particles, respectively (Chen et al., 2024).

These offline methods complement real-time data by resolving molecular-level composition not captured online.

https://doi.org/10.5194/egusphere-2026-4932
Preprint. Discussion started: 10 September 2026

3. Facility Performance and Capabilities

The parameters to be controlled and monitored in the facility are defined by the scientific goals and desired outcomes. The facility must be capable of investigation of i) the emissions from the burning of different fuels, ii) isolation of the emissions from different burn stages, iii) emissions under controlled dilution conditions, iv) transformations of emissions under simulated dark and light atmospheric conditions and v) properties of the emissions that were less suitable for direct flue measurements due to the longer scanning time of the measuring instruments. The Fig. S2, S3, S4, S5, and S6 in Supplementary Information confirm that the facility is able to be used to investigate the different fuels – peat, leaves, hardwood, and softwood, and different dominating burn phases, i.e., smouldering versus flaming. The significantly distinct profiles of the AMS organic-to-SMPS total mass ratio between smouldering and flaming experiments in Fig. S6 further demonstrate the facility's ability to distinguish emissions associated with different combustion phases.

The following subsection, **Subsect. 3.1**, evaluates the operational performance of the facility during biomass-burning experiments involving different fuel types and combustion phases, controlled dilution conditions, and both photoageing and dark-ageing. The evaluated performances include the stability of the relative humidity and temperature, the post-smoke injection mixing times and particle behaviours, the range and consistency of the initial conditions achieved in repeated experiments, and the background cleanliness throughout the experimental campaign that indicate the effectiveness or sufficiency of the applied cleaning procedures. The evolution of the NO and O3 mixing ratios during the biomass-burning experiments, under either photoageing or non-photoageing conditions, along with Leighton Ratio calculations, are in the Supplementary Information (SI), Section 4.

The next subsection, i.e., **Subsect. 3.2.** then demonstrates the scientific capabilities of the facility supported by the range of instrumental measurements of the smoke properties, including those requiring both long scan times and/or extended instrumental duty cycles, under simulated dark and light atmospheric condition simulations. This subsection also includes the facility's capability to support mechanistic analyses of biomass-burning aerosol evolution through the parallel measuring instruments. Other scientific capabilities of this facility are in the last part of the **Subsect. 3.2.**

3.1 Facility Performance and Operational Validation

In this section, the coupled biomass-burning-MAC facility was evaluated in terms of chamber background cleanliness, stability range of environmental control, post-injection smoke mixing time, subsequent particle-concentration behaviour, and the consistency of achieved initial experimental conditions. Overall, the MAC exhibited strong environmental control and cleanliness, supporting consistent and reproducible experimental conditions across campaigns. In general, MAC shows low background PM levels (<1 μg/m³), RH stability at 40–60%, T ~25 °C, stabilized primary gases mixing ratio and PM concentrations within 10–30 min, and a reproducible gas/PM ratio.

https://doi.org/10.5194/egusphere-2026-4932
Preprint. Discussion started: 10 September 2026

3.1.1 Chamber background and environmental control

Background PM level of the MAC was investigated by routine repetition of background experiments (in the current study, 5 times in each of the April and September 2022). The DMPS particle size distribution, total number concentration, total mass concentration, and mode size graphs of each experiment date were provided in Fig. S1**. Figure 2** below shows the SMPS total particle mass concentrations in each background experiment and an example of the PSD of a background experiment. In each experiment, the initial particle mass concentration was consistently below 1 µg/m³ and did not exceed this threshold at any point during the 6 hours of intense illumination (except towards the end of the first background experiment), confirming chamber cleanliness and minimal contamination between runs. The chamber cleaning procedures described in **Sect. 2.1.1** are evidently sufficient, as in Fig.2.a, with only one experiment date that achieved late concentration above 1 µg/m3, which was on 12th April 2025, on which the particle size distribution (PSD) is as in **Fig.2.b.** Based on **Fig.2.b,** there was some evidence of particle formation and growth, likely from condensation of low-volatility organic compounds formed from oxidation of residual organic vapours lost to the walls in previous burning experiments. Whilst contributing to particle number concentration, that modest nucleation mode contributed negligibly to an increase in total particle mass concentration.

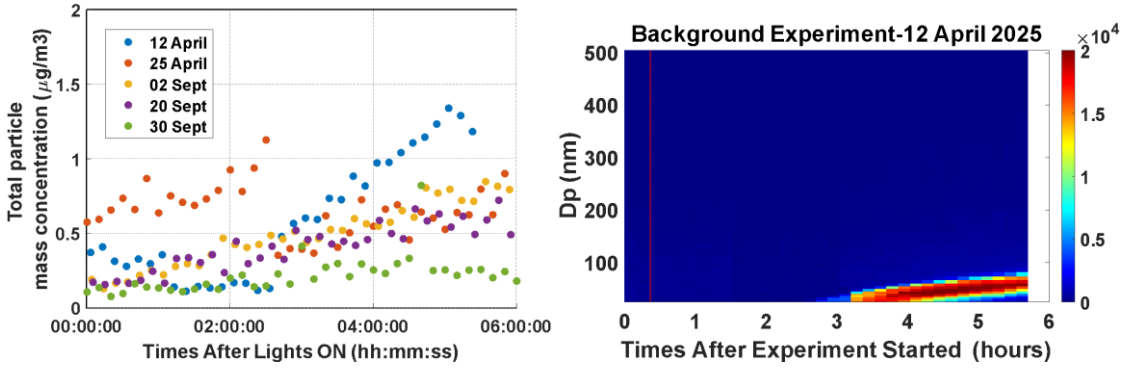

Figure 2: SMPS total particle mass concentrations in background experiments (**a**) and an example of particle size distribution (PSD) of a background experiment (**b**)

Combustion emissions will contribute both heat and moisture to the chamber and hence provide variability to experimental conditions that can influence the measurements**. Figure 3** shows relative humidity (RH) and temperature (T) in the chamber under illuminated (left panels) and dark conditions, with error bars indicating variability across both repetitions and different experiments as listed in Table S1. Noting that the air between the Teflon bag and enclosure is conditioned for both temperature and RH, broadly stable values were achieved after about 1 hour in most experiments of all types. Using setpoints of 25 ˚C and 50%, the stabilized T and RH ranged from 24-26 ˚C, and 40-60%. The control range for T and RH in the chamber and means of adjustment can be found in Shao et al (2022). The individual plots for the experiments can be found in the (Fig. S2, Section SI.3).

https://doi.org/10.5194/egusphere-2026-4932
Preprint. Discussion started: 10 September 2026

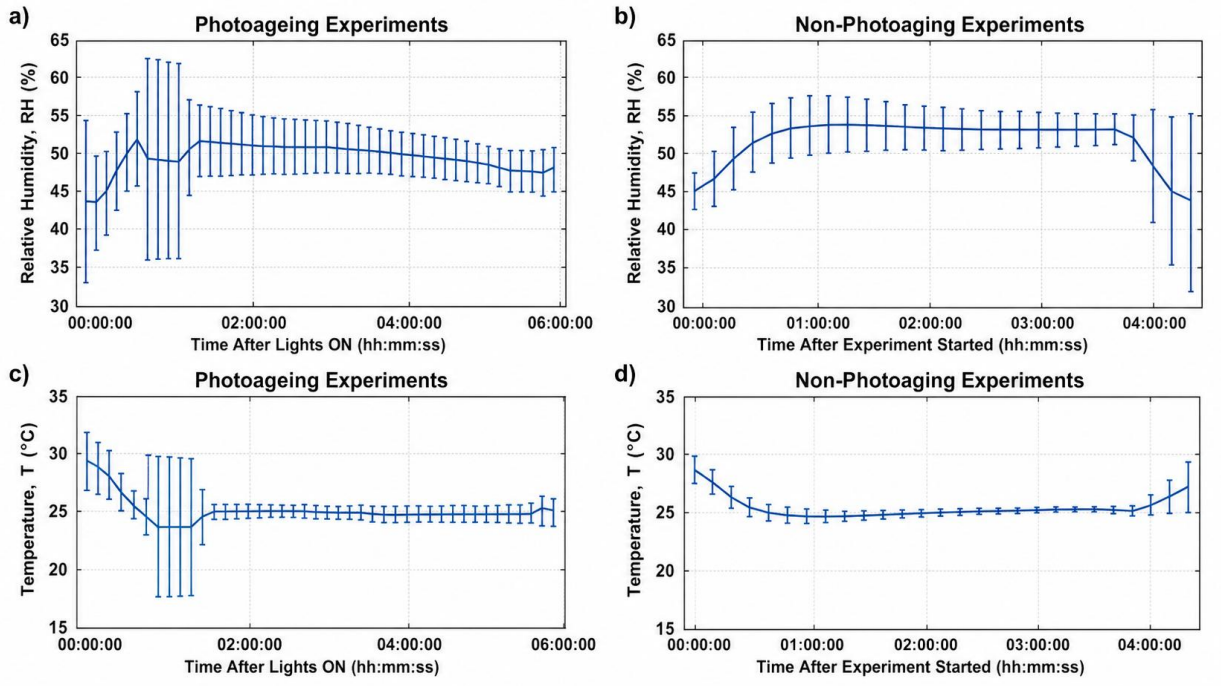

Figure 3: RH and temperature averaged every 10 minutes in photoageing (a, c) and non-photoageing (b, d);

3.1.2. Post-Injection Smoke Mixing Time

Tian et al. (2015) reported a roughly 4-minute equilibration time for injected CO_2 in their 8m^3 dilution chamber. Shao et al. (2022) reported that MAC mixing time based on stabilisation time after injection of NO_2 was on the order of a few minutes. The chamber mixing time investigated using non-acidic ammonium sulphate seed particles was reported as 2.5 minutes based on CPC particle number concentrations. Here, this has been evaluated with components in the smoke emissions using the monitored CO mixing ratio and SMPS particulate matter (PM) concentrations. CO is a primary wood-burning emission and may be considered conservative, which is unreactive on chamber-experiment timescales. They are not seen as produced in sufficient quantities as secondary VOC oxidation products to influence the measured ratios.

Particle number or mass concentrations were also observed since particles may have different complete mixing times in the chamber, compared to the gas mixing time, affected by different wall loss rates. Particles cannot be considered conservative. There are numbers of particle transformation and loss processes that can affect the observed concentrations, in addition to initial mixing and wall loss. Smith et al. (2019) reported that it took between about 60 and 90 minutes for the particle size distribution to stabilise after smoke injection owing to transformation by coagulation, particle growth, and agglomeration. Time required for early stable conditions or trends observed of the particle concentrations may reflect the time needed for both the early or initial (rapid/quick) particle processing/transformations and the achieved completeness of the mixing of the particles.

https://doi.org/10.5194/egusphere-2026-4932
Preprint. Discussion started: 10 September 2026

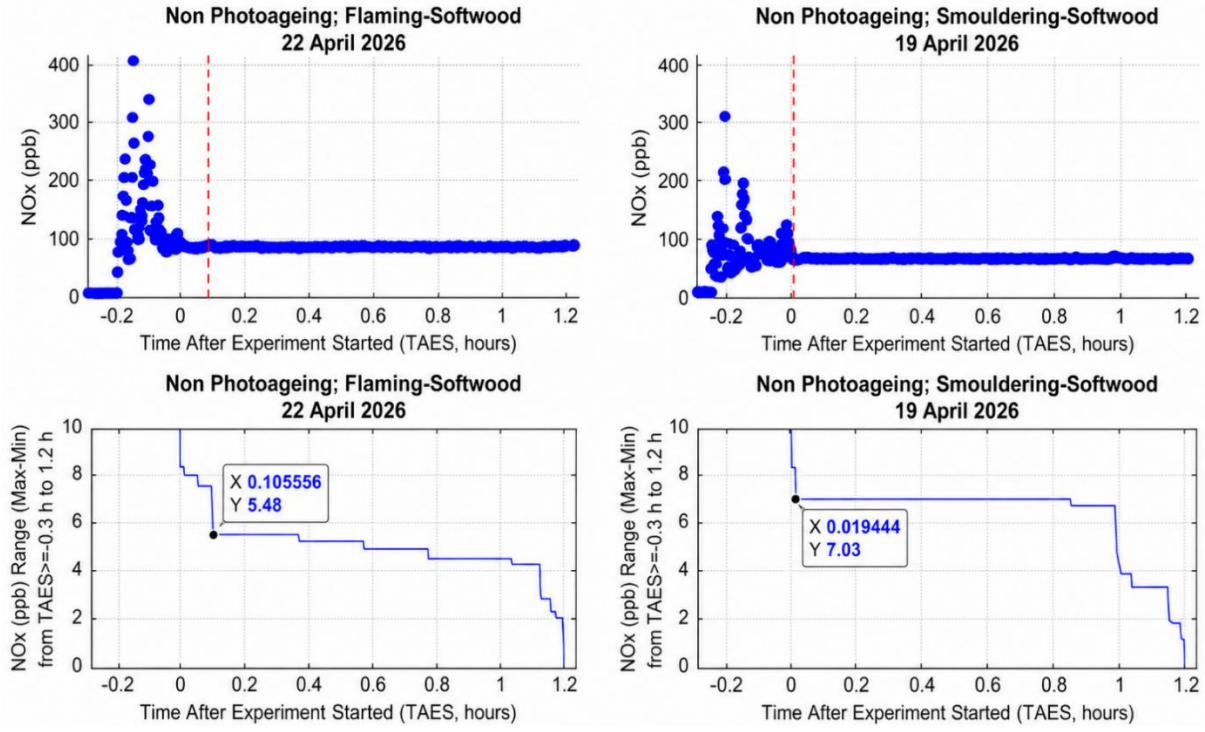

Figure 4: NOx mixing ratio (ppb) at two different non-photoageing experiments: flaming-hardwood on 22 April 2022 (left) and smouldering-hardwood on 19 April 2022 (right); Red dashed lines show the time points at which the concentrations started to stable visually stable: at around 0.1056 hour, i.e. 6.34 minutes (left) and at 0.019 hour, i.e. 1.14 minutes (right) **after the experiment started**, fluctuating for around 5.48 ppb and 7.03 ppb for the largest, respectively. On 19 April, the smoke injection started at 09:41 while the experiment started 15 minutes later at 09:56; Meanwhile, on 22 April, the smoke injection started at 09:47, and the experiment began at 09:58, i.e., 11 minutes later.

Figure 4 shows the NOx mixing ratio values of the two non-photo-ageing experiments. Based on the figures, the NOx mixing ratio seemed to achieve a stable concentration after *no more than* 10 minutes since the first time the mixing system was on, which was right after the completion of the 2nd stage (chamber) dilution, i.e., the start of the experiment. On the other hand, Fig. S3 in the Supplementary Information shows the time series of particle mass concentration (**a**) and particle number concentration (**b**). The SMPS time series particle mass concentration was converted from the size-resolved number concentration and diameter with an assumed uniform density. The particles' stabilization time, in which stable decreases of the particles' concentration were observed, was similarly achieved within 10-30 minutes after the smoke injection or within 0-10 minutes after the experiments started, i.e., after the mixing was on post the completion of the 2nd stage (chamber) dilution.

These smoke particle concentration trends were exceptional for a single experiment, at which some additional emissions, thus additional smoke injection after the start of the experiment, were required to hit the target concentration, like in a softwood-

https://doi.org/10.5194/egusphere-2026-4932
Preprint. Discussion started: 10 September 2026

smouldering experiment on 15 September 2026 (color in red in the 6th (bottom-right panel)) in Fig. S3. The smoke injection continued for about five minutes after the experiment started (cooling was on; chamber filling stopped). In general, the total duration of smoke injection ranged from 2-39 minutes, while the total chamber dilution period ranged from 9-55 minutes.

Based on the roughly equal time required for stabilization of the total particle number concentration and the total particle mass concentration as seen in Fig. S3, it was likely that the particle size distribution was already stable at the time these two total particle concentrations reached a stable condition. Overlaid PM mass concentration time series graphs from each experiment can be found in Fig. S4. **Figure S5** in the Supplementary Information shows the CO-to-SMPS PM mass concentrations. Generally, the CO-to-PM mass ratio increases to varying degrees. It could be an indication of different wall loss rates between these two species and/or different processing since CO is considered as relatively inert while particles are not. Differences in particle wall loss rate in the MAC among different particle sizes have been investigated in Shao et al. (2022). Generally, results in this section demonstrate the effective mixing resulting from the vigorous flow of air-conditioned air around the Teflon bag inside the enclosure. The decision to turn on the lights 40 minutes after the first mixing started in the photoaging experiments, as the start of the photoaging was also already appropriate.

3.1.4. Operating Range and Consistency of Initial Conditions across Repeated Experiments

The target PM mass concentration in this current BB experiments campaign was around 200 µgm-3, while the initial SMPS mass concentration measured in the MAC ranged from 100 to 300 µgm-3, with four experiments being lower than the value range. The initial fraction of SP2-measured Black Carbon (BC) mass from the total PM mass ranged from 0-0.25, with the AMS-measured organic particle mass to SP2-measured BC mass ratio ranging from 0.10 to 19,344.00, covering a wide range of flaming to smouldering combustion. **Table 2** below displays the detailed mean values for each fuel type and each burn phase, including two experiments with initial SMPS PM concentrations below 100 µgm-3: one in F-SW (79 µgm-3) and one in S-SW (31.96 µgm-3). The other two experiments with initial PM concentrations below 100 µgm-3 were excluded due to the unavailability of the data.

Table 2. Consistency of the initial conditions of the repeated hardwood experiments

	Org/PM	BC/PM	Org/BC	O3/PM	NOx/PM	NO/NO2	CO/PM
Flaming-Hardwood	0.05±0.02	0.18±0.04	0.16±0.07	0.11±0.08	0.35±0.15	3.71±1.17	0.02±0.01
Flaming-Softwood	0.06±0.04	0.27±0.12	1.47±1.73	0.13±0.12	0.43±0.21	12.58±14.72	0.03±0.02
Smouldering-Hardwood	0.45±0.14	0.03±0.03	127.4±163.8	0.46±0.21	0.32±0.23	3.66±2.08	0.02±0.01
Smouldering-Softwood	0.82±0.85	0.15±0.16	10.6±8.2	1.01±1.07	0.6±0.6	7.48±6.43	0.09±0.11
Leaves	0.270.11	0.01±0.00	78.08±70.04	0.30±0.14	0.17±0.00	114.46±58.32	0.01±0.01
Peat	0.48±0.05	0.00±0.00	5527.6±1754.8	0.12±0.03	0.15±0.04	159±171.6	0.01±0.00

https://doi.org/10.5194/egusphere-2026-4932
Preprint. Discussion started: 10 September 2026

This dynamic range of initial conditions ensures that the facility characterization presented here covers the necessary potential usage across fuels and conditions, yet is still able to provide sufficient repeatability across the same experiment types as shown in the example below in **Table 3**. **Table 3** shows the consistency of the initial conditions of the repeated hardwood experiments with either smouldering burn phase or flaming burn phase, under either photoaging of non-photoageing conditions. This table illustrates that the experimental setup and design applied in this current biomass burning experimental campaign support sufficient repeatability based on either the Org/PM values or BC/PM values across the same experiment types or repeatability, especially flaming experiments.

Table 3. Consistency of the initial conditions of the repeated hardwood experiments

	Org/PM	BC/PM	Org/BC	O3/PM	NOx/PM	NO/NO2	CO/PM
Non Photoageing Flaming							
22-Apr	0.02	0.17	0.14	0.12	0.46	3.51	0.01
29-Apr	0.02	N/R	N/R	0.15	0.20	2.83	0.02
Non Photoageing Smouldering							
19-Apr	0.20	0.04	4.62	0.47	0.36	1.09	0.03
27-Apr	0.27	0	74.92	0.32	0.08	3.04	0.02
Flaming							
21-Apr	0.02	0.14	0.11	0.13	0.32	2.25	0.02
28-Apr	0.02	0.19	0.10	0.08	0.26	5.11	0.03
30-Aug	N/R	N/R	N/R	N/R	N/R	2.81	N/R
22-Sep	0.06	0.19	0.33	0.06	0.36	3.75	0.009
Smouldering							
20-Apr	0.21	0.02	9.88	0.34	0.20	1.51	0.02
26-Apr	0.24	0.00	168.51	0.20	0.04	3.70	0.01
31-Aug	0.30	0.07	4.31	0.75	0.62	6.20	0.04

3.2. Scientific Capabilities of the Facility

3.2.1 Ability to measure parameters inaccessible to direct exhaust measurement owing to low instrument duty cycles

Owing to the suite of fast online instrumentation coupled to the MAC, many of the parameters shown above and measured by instruments listed in **Sect. 2.2** could be measured directly from the flue (possibly diluted). However, many parameters require a longer time resolution owing to the scanning time of the instruments. Additionally, they can also require a long duty cycle due to either the complexity of the particles or the data processing method itself. Examples are particle size distributions measured by DMPS, as well as subsaturated and supersaturated hygroscopicity measured by HTDMA and CCNc, respectively, which both can require 1 hour for a single full cycle of the 10-minute measurement points. Meanwhile, the smoke generation process for certain amounts of fuel in a typical combustion source, especially flaming combustion, normally lasts for only about less than 10-minutes or requires a continuous supply of fuel. Besides, direct measurements of the flowing smoke, while requiring a long scan time (e.g., 10 minutes) for one measurement point, can be quite challenging due to the large variability of transient

https://doi.org/10.5194/egusphere-2026-4932
Preprint. Discussion started: 10 September 2026

emissions. The coupling of the combustion source with MAC helps to overcome this challenge by collecting enough smoke mixed uniformly in the chamber, so that not only one scan or one cycle of measurements can be achieved, but longer measurement time can still be accommodated. Therefore, a set of repetitions can be obtained instead of a single observation only – though any dilution, mixing, and dark physicochemical processing effects during the measurements may influence the resulting properties slightly.

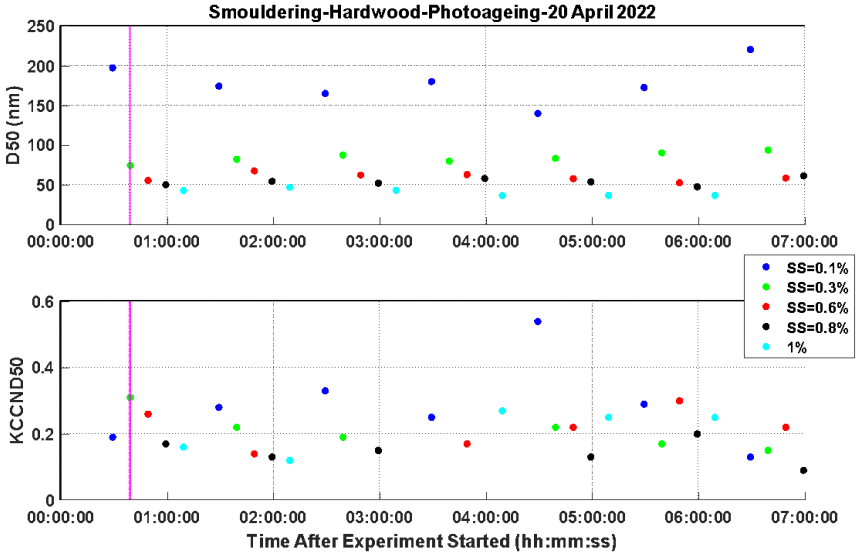

Figure 5: A 10-minute resolution time series curve of D50 values (above panel) and a 10-minute resolution time series curve of KCCND50 values (below panel) at 5 different tested supersaturation values. The vertical line shows the lights on.

Figure 5 above shows both a 10-minute resolution time series curve of D50 values (above panel) and a 10-minute resolution time series curve of D50 values (below panel) at 5 different tested supersaturation (SS) values. The measurement started from the lowest SS value, which is 0.1%, then moved to the next higher SS until the highest SS, at which each SS level took roughly 10 minutes in total to finish its full particle size scan. Once the highest SS level scan was finished, the measurement was returned to the lowest tested SS level. Additionally, in each loop of the SS scan, the measurement at the lowest SS was conducted twice. The 1st one is to allow stabilization of the SS after moving from the highest SS. However, in the data processing, the 1st lowest SS measurement was not used – just as in **Fig. 9** above, in which there were parts where the gap was 20 minutes instead of 10 minutes. Activation fraction, F_A, curves of each supersaturation and time point where the D50 and KCCND50 values were derived can be seen in Fig. S7, SI.3. In this figure, as the smouldering hardwood emissions were photo-aged the size dependent AF values shift much bigger to the lower diameter sizes with the increase of supersaturation values, while the time series did not change the AF curves as much as the applied changes of the supersaturation conditions. The long duty cycle for the combined DMA-CCNc results in scans across all particle sizes and all supersaturations in one hour.

https://doi.org/10.5194/egusphere-2026-4932
Preprint. Discussion started: 10 September 2026

Figure 6 illustrates subsaturated hygroscopicity determined by HTDMA over a similarly extended sampling period. The instrument stepped through all dry and wet sizes to derive a full sub-saturated hygroscopicity profile of the particles in a one-hour duty cycle (as outlined in **Sect. 2.2.3**).

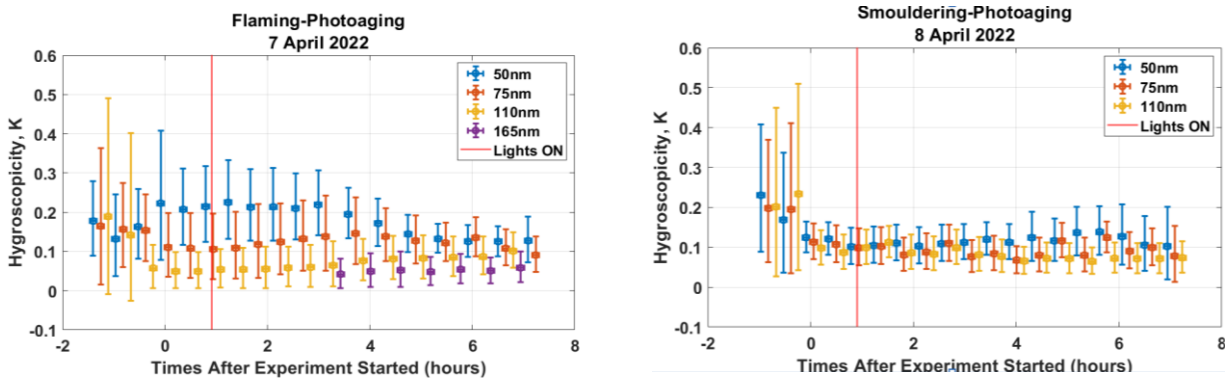

Figure 6: HTDMA hygroscopic parameter, kappa (κ), in softwood flaming (left) and smouldering (right) experiments on 7th April 2022 and 8th April 2022, respectively. Error bars correspond to measurement data point error

Owing to the burn variability and associated transients, measurements such as those from the HTDMA and DMA-CCNc would be impossible were the instruments sampling emissions directly from the flue.

3.2.2. Ability to contrast transformations of emissions under different simulated atmospheric conditions

Even though direct flue measurements are beneficial for more accurate or direct MCE and emission inventory calculation of primary pollutants, they are not able to reveal the transformations that these emissions would experience under atmospheric physical or chemical processing. Transformations will follow changes in environmental conditions after emission, including through physical drivers such as dilution, cooling and changes in RH. They may also occur as a result of chemistry driven by daytime or night-time oxidants. It is therefore necessary to conduct some kind of conditioning after emission and before measurement under the desired conditions. The MAC facility is well-suited to conduct photochemical and dark-ageing experiments by diluting and holding known concentrations from the woodsmoke under controlled dark or illuminated conditions. The evolution of NO mixing ratio and O3 ratio mixing ratio along with its discussion is provided in Supplementary Information Section 4, S.I.4.

It is clear that photochemical transformations of woodburning emissions can be explored in the combined MAC facility, and that online instrumentation can readily capture their evolution over time. Similarly, the impact of coupled photochemical and microphysical transformations on the size distribution of the PM emissions can be directly observed as shown in **Fig. 7.** This shows the evolution of the initially bimodal size distribution of softwood flaming smoke emissions under a) dark and b)

https://doi.org/10.5194/egusphere-2026-4932
Preprint. Discussion started: 10 September 2026

illuminated experiments as measured by SMPS. The contour panels in the top row show the particle number distributions from 14 nm to 661 nm, with hotter colours indicating higher concentrations. The second row shows the number-weighted mean of the particle diameter (nm). There is an indication of a more significant formation of a smaller new particle mode in the illuminated experiment, reducing the mean size later in the experiment in comparison to that in the dark experiment.

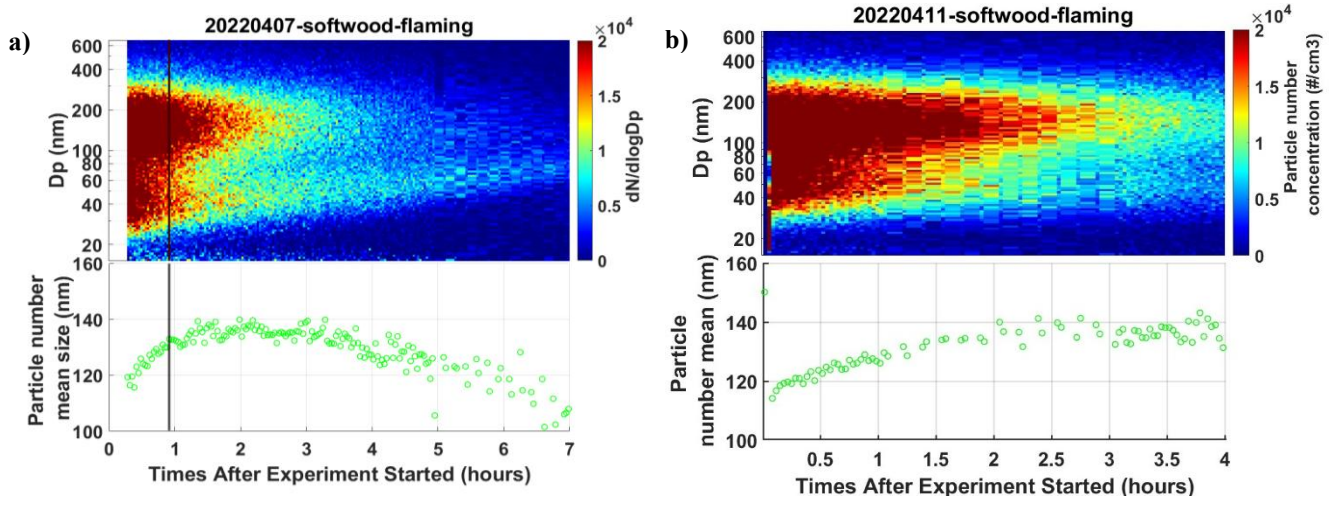

Fig 7 SMPS size distribution graphs of smoke particles under dark ageing (a) and photo-ageing (b) conditions; black vertical line indicates the time of lights on, i.e., start of the photoaging

3.2.3 Illustrative Capability to Conduct Multiparameter Analysis Supporting Future Mechanistic Study I: Of Cloud-Related Properties

The extended MAC facility is able to explore changes in the properties of the fuel burning emissions sampled from a specified burn phase in stove, as they are transformed under specified and controlled conditions in the MAC. This section aims to illustrate the facility's capability in supporting any future mechanistic study of particles' property evolution through the conducted time series multiparameter analysis gained from the parallel continuous multi-instruments' measurement. Specifically, this current section briefly demonstrates how the parallel continuous measurements of particle size distribution (PSD) and chemical compositions through both AMS measurements and SP2 measurements can help in understanding the contrasted values and trends of the photoaging driven changes of the HTDMA subsaturated hygroscopicity values from smouldering and flaming experiments of the same fuel type, as observed in **Fig. 8** in **Sec. 3.2.1.** Measurements from the flaming phase experiment are displayed in the left column of panels, while those from a comparable smouldering experiment are in the right column in **Fig. 8** below. This section is for illustrative purposes only, not for a full scientific investigation and discussion of a multiparameter or mechanistic study.

https://doi.org/10.5194/egusphere-2026-4932
Preprint. Discussion started: 10 September 2026

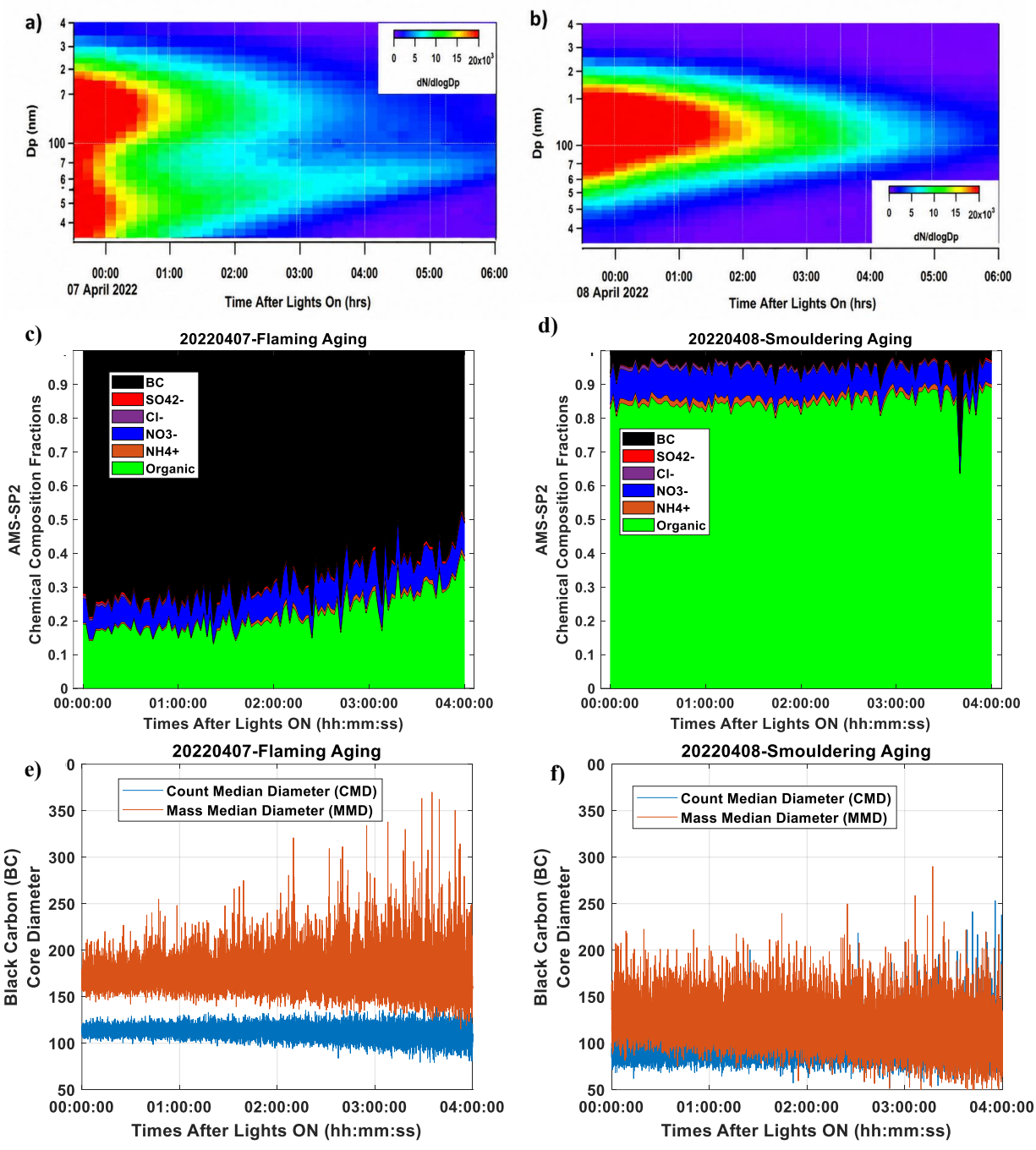

Figure 8: Graphs of the parallel and continuous time series measurements of **a**) DMPS sub-micrometer particle size distributions and **b**) AMS component fractions, **c**) Black carbon (BC) core count median diameter (CMD) and mass median diameter (MMD) time, contrasting a flaming softwood (**F-SW-1**) and a smouldering softwood experiment (**S-SW-1**) on 7th April 2022 and 8th April 2022, respectively.

https://doi.org/10.5194/egusphere-2026-4932
Preprint. Discussion started: 10 September 2026

Both particle size distribution and chemical composition are key determinants of certain important impact-related parameters, such as hygroscopicity and optical properties. **Figure 8** shows the results from two instruments of the driving properties, comparing flaming and smouldering experiments of softwood (F-SW-1 and S-SW-1, respectively). Based on **Fig. 8**, the DMPS particle size distribution graphs in **Fig. 8.a** showed a bimodal distribution in the flaming experiment, whereas a unimodal distribution in the smouldering experiment, peaking at the larger size. Meanwhile, **Fig. 8.b** showed both a higher bulk inorganic: organic ratio and higher bulk black carbon (BC) content in the flaming experiment than in the smouldering experiment of the same wood type. The different combinations of the PSD and chemical composition characteristics of particles emitted from the different burn phases lead to different characteristics of the affected or driven properties like HTDMA sub-hygroscopicity, as seen in **Fig. 6**.

Obvious strong size-dependence of the HTDMA hygroscopicity parameter (κ) values were observed in the flaming-07 April 2022 experiment, suggesting both different chemical compositions of particles in the first peak and those in second peak of the experiment's bimodal PSD and higher presence of BC in the larger particles keeping the hygroscopicity values at thoses sizes low. The BC core sizes were confirmed in Fig. **8.c**. The count median diameter (CMD) of the BC core started at around 100-120 nm in the early beginning of the flaming photoageing experiment. Meanwhile, the low amounts of BC contained in the smouldering particles started their core CMD values at both lower and wider, at around 70-110 nm, suggesting a likely less size dependence of the bulk particles' chemical composition. Additionally, by considering change in the particle size distribution in **Fig. 8.a.** of the bulk particles, the decreasing trend of the hygroscopicity at 50 nm in the flaming experiment-07 April 2022 may actually not represent ageing driven evolution of the same particles. It could possibly indicate external mixing presence of the particles since the beginning, leaving only the less dominating fraction of particles with lower hygroscopicity upon ageing while the dominating fraction with higher hygroscopicity agglomerated or grew into bigger sizes. More thorough investigation of the HTDMA fitting graphs should be able to confirm the presence or absence of the observed mixing conditions of the hygroscopic growth factors at each particle size. Moreover, time evolution of BC coating thickness from SP2 measurements and size-resolved chemical composition from SP2-AMS measurements could likely provide useful information to either support or dis-support the hypothesis of the organic condensation to the existing particles. The widening part of the low sizes of the BC core diameter to achieve lower sizes, i.e. slight decreasing tendency upon ageing may be caused by slight restructuring of the BC contained in some fraction of the black carbon-containing particles. All these comparisons illustrate the benefits of the presence of online parallel measuring instruments in the facility, thereby enabling the facility to investigate the driving factors of certain parameters, while importantly monitoring the upon ageing time evolution with added capability in contrasting different burn phases and fuel types.

A full scientific investigation of hygroscopicity and the driving properties is in an under-review paper (Syafira et al 2026). Meanwhile, an investigation of the ice-nucleation ability of the filtered sample particles, which is connected to their chemical composition, is published in an article by Chen et al., (2025). Additional brief illustration, which was of optical properties, is

https://doi.org/10.5194/egusphere-2026-4932
Preprint. Discussion started: 10 September 2026

in the **Supplementary Information, Sect. S5.** In that section, black carbon was seen as clearly higher in flaming (07 April 2022), leading to a much lower OC:BC ratio in the flaming experiment than in the smouldering experiment (08 April 2022) of the same fuel type. It was also then clear that absorption of the total absorption was higher in the same flaming experiment due to the high BC content, yet the scattering was higher in the smouldering experiment. Black carbon is known as a component with high absorption across the infrared, visible, and ultraviolet regions (**Liu et al., 2019**).

3.2.4. Other Possible Scientific Capabilities

Figure S8 shows the aerodynamic size distribution of particles ranging from 0.5- 20 μm of a flaming hardwood burning experiment compared to a smouldering hardwood burning experiment on 21 April 2022 (**F-HW-1**) and 20 April 2022 (**S-HW-2**), respectively. This information can add to the comprehensive understanding of the biomass burning particles under investigation and how they differ under different burning conditions and different fuel types.

In addition to the comparisons among several key or important particle properties, multi-instruments installation has been also beneficial due to presence of primary gases measurements to investigate possible chemical processes behind the particle properties' transformation. This was done by Evan et al., 2024; and Evan et al., 2025, utilizing the time-evolution data for the primary gases and for both the AMS and SP2 online time-series chemical composition analyses to support their investigation on the detailed offline chemical composition investigation of both fresh and aged filtered particles. Online mass spectrometry analysis provided by the FIGERO-CIMS measurements can provide real-time gas-phase composition (and near real-time particle-phase). Two published articles regarding this are in Oghama et al., 2025 and Oghama et al., 2026. Lastly, the installation of a thermodenuder can provide particle volatility data to complement chemical composition data.

Overall, the presence of a heavily instrumented chamber at the University of Manchester biomass burning aerosol study facility enables a wide range of advanced investigations. The setup supports continuous, parallel measurement of gas- and particle-phase properties, making it ideal for studies exploring relationships between emission composition, hygroscopicity, optical properties, volatility, and aging behaviour. Mechanistic studies can be performed across different stages of smoke evolution — from fresh emissions to dark- or photo-aged aerosols — allowing researchers to isolate the impact of specific variables. For example, the effects of certain parameters at initial conditions on the ageing processes can be systematically tested. Besides, though oxidant addition and humidity modulation were not implemented in the initial campaign, the facility is already configured to support such experiments. Together, these capabilities enable high-resolution, multiparametric studies that bridge the gap between field realism and laboratory control.

https://doi.org/10.5194/egusphere-2026-4932
Preprint. Discussion started: 10 September 2026

4. Recommendations for Improvements

Repeatability of the initial CO (ppb) to SMPS mass concentration ratio values might be able to give insight on the repeatability of the sampling-injection-dilution system that should be able to be better accomplished through a more accurate calculated dilution ratio monitoring presence. That could be done by including CO gases measurement at both the exhaust stack during the smoke injection and at the chamber at the start of the experiment. The dilution ratios could then be used to observe the consistency or repeatability of the sampling-injection-dilution system as follows.

Suppose the particle concentrations at the source were similar. In that case, unchanged settings of the sampling-injection-dilution system resulting in same dilution ratios of the produced CO should be able to lead to the same initial particle mass concentrations at the chamber. Meanwhile, changing the CO dilution ratio through an adjustment on the sampling-injection-dilution system while the initial particle concentrations at stack were similar should lead to proportionally different initial particle concentrations in the chamber. Calculation could then be conducted to obtain how proportionally the CO dilution ratio affects the PM concentration dilution ratio. After that, when the particle concentrations at the stack were different, an applied adjustment in the sampling-injection-dilution system to achieve the calculation based required CO dilution ratio value, should still be able to lead to similar initial particle concentrations in the chamber with same smoke injection duration. If that effort does not lead to similar initial particle concentrations, an investigation might need to be conducted on the sampling-injection-dilution system questioning the repeatability of the system. Clogging might occur in the line reducing the flow of the particles and changing the initial particles to gases ratio, though it might be able to detect intuitively through observation on duration of the smoke injection needed to achieve the intended initial particle concentration when roughly similar concentrations at stack were still observed.

Furthermore, an effort to measure the total initial gas phases of the smoke, including the organic gases, at both the exhaust stack and the chamber could even possibly add more confidence in investigating the consistency of the used sampling-injection-dilution system across the experiments. The comprehensive measurement of the initial gases' phases of the smoke at the start of the experiment would likely be beneficial too to have a better understanding on factors that affect the initial properties of the particles and their changes during either the photoaging or non-photoaging.

The other procedural suggestion that should be considered for the next biomass burning study at the facility was applying a more similar time duration of the preceding dark measurements period of the photoaging experiments to increase the similarity of the initial conditions at the time that the lights were on across experiments. Importantly, the start and the end of the initial dark measurement should possibly also consider the time required for stabilization of the RH and T measurements, particles concentration, and gases mixing ratio in the chamber since the end of both the smoke injection and chamber (2^{nd} stage) dilution.

https://doi.org/10.5194/egusphere-2026-4932
Preprint. Discussion started: 10 September 2026

Lastly, it would probably be beneficial too if there was data of the ambient air pulled into the chamber during the two different seasons, i.e., April and September, to be measured and compared to each other. This was because the biomass burning was done outside the laboratory building using the surrounding ambient air to burn the fuels in the stove. Though this was beneficial in terms of generating more open-burning representative combustion, any differences in the measurement results conducted at the different seasons should probably be checked to see whether the difference was also caused by the possibly different ambient air conditions at the different seasons or whether the difference was just actually showing the different background values of those different seasons. For example, the ambient air condition during the flaming-hardwood experiment on April 21, 2022, can be roughly estimated by checking the ambient air at Manchester Supersite with data displayed at http://whitworth.cas.manchester.ac.uk/firs/2022/04/21/. Meanwhile, on September 22, 2022, data can be checked at http://whitworth.cas.manchester.ac.uk/firs/2022/09/22/

Conclusion

This study presents a new laboratory facility that integrates a wood-burning stove with the Manchester Aerosol Chamber (MAC), enabling controlled, repeatable investigations of biomass burning emissions and their transformation under both dark and photochemical conditions. Demonstrated capabilities include clear differentiation of emission profiles by fuel type and combustion phase, reproducible contrasts between photoaging and non-photoaging pathways with possible addition of injected oxidants, as well as integration of CCNc, HTDMA, optical properties, size distribution, and high-resolution chemical composition measurements for advanced aerosol characterization. This facility enables detailed mechanistic studies or multiparameter analytical studies of biomass-burning aerosol evolution, bridging the gap between simple oxidation flow reactors and complex ambient field campaigns. The facility shows low background PM levels, typically less than 1 $\mu g/m^3$, confirming the sufficiency of currently applied cleaning procedures and frequency. The temperature and RH stabilized at around 24-26 °C and 40-60% during the biomass burning experiments once set to T=25 °C and RH=50%. Meanwhile, gases and particles, each, seemed to stabilize or mixed uniformly, within less than 10–30 minutes after both smoke injection and dilution.

Code and data availability

The code and data are available at Zenodo: https://doi.org/10.5281/zenodo.22108209

Supplement link

The link to the supplement will be included by Copernicus.

https://doi.org/10.5194/egusphere-2026-4932
Preprint. Discussion started: 10 September 2026

Author contributions

DH, AV, JA, GM, HC designed the whole biomass burning facility. **DH, AV, GC** designed and constructed the stove-chamber connection and 1st stage dilution. **GM** installed the stove oven and flue in the trailer and made all connections to the flue. **AV** designed and constructed the exhaust fresh emission particle sampling filter connection. **AV, OO, SAS**, did the other setups, e.g. thermodenuder setups, instruments' connection setup, gas instruments' calibrations, background experiments, and cleaning experiments. **SAS, OO, AV, HH, YS** did the daily main experiments during April and September 2022 and shared responsibilities for the instruments' operation, calibration, and raw data management. **SAS** and **HH** shared responsibilities for the raw main and calibration data processing. **RE, JC, YW, and OO** joined some experiments and did both fresh- and aged-particle sample collections. **OO** took responsibility for the daily running of CIMS and its data product. **SAS** took responsibility for the final quality-assured and shareable processed data of the online instruments in the facility, except PASS and CIMS. **SAS** prepared all of the graphs using the available processed data and wrote the manuscript with inputs from all authors. **AV** and **GM** did significant cuts for efficiency on the 1st completed draft version of this article. **PG, JA, HC, GM, and AV** did the managerial aspects of this project. **MF** provided technical support.

Competing interests

The authors declare that they have no conflict of interest.

Disclaimer

Copernicus Publications remains neutral with regard to jurisdictional claims made in the text, published maps, institutional affiliations, or any other geographical representation in this paper. While Copernicus Publications makes every effort to include appropriate place names, the final responsibility lies with the authors. Views expressed in the text are those of the authors and do not necessarily reflect the views of the publisher.

Acknowledgements

We acknowledge the use of ChatGPT Plus for figure quality improvement with careful use and/or comparison for Figure 1, Figure 3, Figure 4, and Figure 8a), with the prompt "improve quality, but exactly same graphs". The initial figures can be checked in the Zenodo link. https://doi.org/10.5281/zenodo.22108209

https://doi.org/10.5194/egusphere-2026-4932
Preprint. Discussion started: 10 September 2026

Financial support

The Manchester Aerosol Chamber receives funding from the Horizon 2020 Research and Innovation Framework Programme, H2020-INFRAIA-2020-1, Sustainable Access to Atmospheric Research Facilities (ATMO-ACCESS) (grant agreement no. 101008004). **Sara Aisyah Syafira** acknowledges studentship support from the Indonesia Endowment Fund for Education (Lembaga Pengelola Dana Pendidikan, LPDP) with sponsorship reference number LOG-1962/LPDP.3/2023, and **Osayomwanbor Oghama** acknowledges studentship support from the Tertiary Education Trust Fund (TETFund), Nigeria, with sponsorship reference number TETF/ES/UNIV/DELTA STATE/TSAS/2019. **Aristeidis Voliotis** acknowledges funding support from the Natural Environment Research Council (NERC) through the UK National Centre for Atmospheric Science (NCAS).

References

Bannan, T. J., Percival, C. J., Priestley, M., et al.: Using advanced mass spectrometry to investigate the oxidation of biogenic VOCs and their role in new particle formation, Atmos. Chem. Phys., 19, 123–142, https://doi.org/10.5194/acp-19-123-2019, 2019.

Bertrand, A., et al.: Influence of fuel moisture content and combustion conditions on emissions of trace gases and particles from laboratory combustion of wildland fuels, Atmos. Chem. Phys., 17, 7325–7340, https://doi.org/10.5194/acp-17-7325-2017, 2017.

Chen, Y., et al.: Chemical characterization of fresh and aged biomass burning emissions using high-resolution time-of-flight aerosol mass spectrometry, Atmos. Chem. Phys., 16, 11013–11032, https://doi.org/10.5194/acp-16-11013-2016, 2016.

Chen, J., Jakob, F. M. O., Voliotis, A., Wu, H., Syafira, S. A., Oghama, O., Shardt, N., Fauré, N., Kong, X., McFiggans, G., and Kanji, Z. A.: Ice nucleation abilities and chemical characteristics of laboratory-generated and aged biomass burning aerosols, Environ. Sci. Technol., 59, 2575–2586, https://doi.org/10.1021/acs.est.4c04941, 2025.

Ching, J., Adachi, K., Zaizen, Y., Igarashi, Y., and Kajino, M.: Aerosol mixing state revealed by transmission electron microscopy pertaining to cloud formation and human airway deposition, npj Clim. Atmos. Sci., 2, 22, https://doi.org/10.1038/s41612-019-0081-9, 2019.

Corbin, J. C., Sierau, B., Gysel, M., Laborde, M., Keller, A., Kim, J., Petzold, A., Onasch, T. B., Lohmann, U., and Mensah, A. A.: Mass spectrometry of refractory black carbon particles from six sources: carbon-cluster and oxygenated ions, Atmos. Chem. Phys., 14, 2591–2603, https://doi.org/10.5194/acp-14-2591-2014, 2014.

Coggon, M. M., et al.: Volatile organic compound emissions from biomass burning derived from airborne measurements during FIREX, Atmos. Chem. Phys., 19, 8529–8546, https://doi.org/10.5194/acp-19-8529-2019, 2019.

Engelhart, G. J., et al.: Cloud condensation nuclei activity of fresh primary and aged biomass burning aerosol, Atmos. Chem. Phys., 12, 7285–7293, https://doi.org/10.5194/acp-12-7285-2012, 2012.

https://doi.org/10.5194/egusphere-2026-4932
Preprint. Discussion started: 10 September 2026

589 Evans, M. J., et al.: Model evaluation of regional aerosol-cloud-radiation interactions during biomass burning events, Atmos.
590 Chem. Phys., in press, 2024.
591 Evans, R. L., Bryant, D. J., Voliotis, A., Hu, D., Wu, H., Syafira, S. A., Oghama, O. E., McFiggans, G., Hamilton, J. F., and
592 Rickard, A. R.: A semi-quantitative approach to nontarget compositional analysis of complex samples, Anal. Chem., 96,
593 18349–18358, https://doi.org/10.1021/acs.analchem.4c00819, 2024.
594 Evans, R. L., Bryant, D. J., Voliotis, A., Hu, D., Wu, H., Syafira, S. A., Oghama, O. E., McFiggans, G., Hamilton, J. F., and
595 Rickard, A. R.: The importance of burning conditions on the composition of domestic biomass-burning organic aerosol
596 and the impact of atmospheric ageing, Atmos. Chem. Phys., 25, 4367–4389, https://doi.org/10.5194/acp-25-4367-2025,
597 2025.
598 Grieshop, A. P., Logue, J. M., Donahue, N. M., and Robinson, A. L.: Laboratory investigation of photochemical oxidation of
599 organic aerosol from wood fires 1: measurement and simulation of organic aerosol evolution, Atmos. Chem. Phys., 9,
600 1263–1277, https://doi.org/10.5194/acp-9-1263-2009, 2009.
601 Haslett, S. L., et al.: Composition and properties of fresh and aged biomass burning aerosol from Canadian boreal forest fires,
602 Atmos. Chem. Phys., 18, 10915–10930, https://doi.org/10.5194/acp-18-10915-2018, 2018.
603 Hatch, L. E., Yokelson, R. J., Stockwell, C. E., Veres, P. R., Simpson, I. J., Blake, D. R., Orlando, J. J., and Barsanti, K. C.:
604 Multi-instrument comparison and compilation of non-methane organic gas emissions from biomass burning and
605 implications for smoke-derived secondary organic aerosol precursors, Atmos. Chem. Phys., 17, 1471–1489,
606 https://doi.org/10.5194/acp-17-1471-2017, 2017.
607 Hennigan, C. J., et al.: Chemical and physical transformations of organic aerosol from the photo-oxidation of biomass-burning
608 emissions, Atmos. Chem. Phys., 11, 7669–7686, https://doi.org/10.5194/acp-11-7669-2011, 2011.
609 Hodshire, A. L., et al.: Aging effects on biomass burning aerosol size distributions: a synthesis of field data and implications for
610 modelling, Atmos. Chem. Phys., 19, 10965–10981, https://doi.org/10.5194/acp-19-10965-2019, 2019.
611 Hoi, K.-C., et al.: Chemical characterization and radiative properties of urban and biomass burning aerosols during winter haze
612 in Asia, Atmos. Environ., 78, 202–210, https://doi.org/10.1016/j.atmosenv.2012.03.025, 2013.
613 Iraci, L. T., et al.: Constraints on black carbon emissions and aging from FIREX-AQ field observations, Atmos. Chem. Phys.,
614 22, 6781–6800, https://doi.org/10.5194/acp-22-6781-2022, 2022.
615 Kong, W., et al.: Optical properties of aged biomass burning aerosol during long-range transport, Atmos. Chem. Phys., 21,
616 14569–14589, https://doi.org/10.5194/acp-21-14569-2021, 2021.
617 Leighton, P. A.: Photochemistry of Air Pollution, Academic Press, 1961.
618 Leskinen, A., et al.: Emission and transformation of SOA precursors from wood combustion, Atmos. Environ., 119, 418–425,
619 https://doi.org/10.1016/j.atmosenv.2015.08.031, 2015.
620 Levin, E. J. T., et al.: Aerosol chemical composition of aged biomass burning emissions from boreal forest fires in the Eastern
621 Canadian Arctic, Atmos. Chem. Phys., 10, 9729–9742, https://doi.org/10.5194/acp-10-9729-2010, 2010.

https://doi.org/10.5194/egusphere-2026-4932
Preprint. Discussion started: 10 September 2026

Lien, J. and Hung, H.-M.: Kinetic studies on biomass burning aerosol–water interactions, Environ. Sci. Technol., 55, 8450–8458, https://doi.org/10.1021/acs.est.1c01234, 2021.

Liu, F., et al.: Secondary organic aerosol formation from the aging of biomass burning emissions, Environ. Sci. Technol., 53, 7796–7805, https://doi.org/10.1021/acs.est.9b01184, 2019.

Long, R. W., et al.: Ambient measurement of biomass burning aerosols in western U.S. wildfire plumes, Atmos. Environ., 262, 118608, https://doi.org/10.1016/j.atmosenv.2021.118608, 2021.

Marsavin, A., et al.: The photochemical aging of brown carbon aerosols and implications for climate, Environ. Sci.: Atmos., 3, 1204–1218, https://doi.org/10.1039/D3EA00043A, 2023.

McMeeking, G. R., et al.: Emissions of trace gases and aerosols during open biomass burning in the western U.S., J. Geophys. Res., 114, D13303, https://doi.org/10.1029/2008JD011532, 2009.

Oghama, O. E., Voliotis, A., Bannan, T. J., Syafira, S. A., Hu, D., Wu, H., Gallimore, P., McFiggans, G., Coe, H., and Allan, J. D.: Variations in oxygenated and nitrogen-containing primary organic compounds based on the fuel type and burning condition in stove emissions, Environ. Sci.: Atmos., 5, 1297, https://doi.org/10.1039/d5ea00080g, 2025.

Oghama, O. E., Voliotis, A., Bannan, T. J., Syafira, S. A., Hu, D., Wu, H., Gallimore, P., Matthews, E., McFiggans, G., Coe, H., and Allan, J. D.: Effect of photochemical aging on biomass burning emissions: contributions of oxidized organic nitrogen from a variety of biomass types, ACS Earth Space Chem., 10, 1626–1640, https://doi.org/10.1021/acsearthspacechem.6c00093, 2026

Ortega, A. M., et al.: Secondary organic aerosol formation and aging from combustion emissions, Atmos. Chem. Phys., 13, 11551–11571, https://doi.org/10.5194/acp-13-11551-2013, 2013.

Patoulias, D., et al.: Modeling wildfire plumes and chemical transformations in the eastern Mediterranean, Atmosphere, 12, 1458, https://doi.org/10.3390/atmos12111458, 2021.

Priestley, M., et al.: The effect of atmospheric aging on the physicochemical properties of biomass burning aerosol, Atmos. Chem. Phys., 18, 4561–4578, https://doi.org/10.5194/acp-18-4561-2018, 2018.

Price-Allison, A., et al.: Influence of chemical composition on the cloud condensation nuclei activity of biomass burning aerosol, Atmos. Chem. Phys., 19, 13973–13990, https://doi.org/10.5194/acp-19-13973-2019, 2019.

Price-Allison, A., et al.: Cloud microphysical impacts of different biomass burning aerosol types, Atmos. Environ., 284, 119295, https://doi.org/10.1016/j.atmosenv.2022.119295, 2023.

Rein, G. and Huang, X.: Smouldering combustion and its role in wildfires and climate, Philos. Trans. R. Soc. B, 376, 20200370, https://doi.org/10.1098/rstb.2020.0370, 2021.

Roson, R., et al.: Modeling economic and health impacts of wildfire smoke in Europe, Sci. Total Environ., 776, 145959, https://doi.org/10.1016/j.scitotenv.2021.145959, 2021.

Shao, L., et al.: Size-resolved chemical composition and toxicity of biomass burning aerosol, Environ. Pollut., 305, 119269, https://doi.org/10.1016/j.envpol.2022.119269, 2022.

https://doi.org/10.5194/egusphere-2026-4932
Preprint. Discussion started: 10 September 2026

Smith, J. D., et al.: Cloud droplet activation and CCN activity of aged biomass burning particles, Atmos. Chem. Phys., 19, 12021–12034, https://doi.org/10.5194/acp-19-12021-2019, 2019.

Solomon, P. A., et al.: Wildfire smoke and health: current knowledge and future needs, Environ. Sci. Technol., 56, 10290–10305, https://doi.org/10.1021/acs.est.2c00905, 2022.

Stockwell, C. E., et al.: Characterization of biomass burning emissions from cooking fires and other sources using PTR-TOF-MS, Atmos. Chem. Phys., 15, 845–865, https://doi.org/10.5194/acp-15-845-2015, 2015.

Stockwell, C. E., et al.: Airborne emission rate measurements validate remote sensing observations and emission inventories of wildfires, Environ. Sci. Technol., 56, 7564–7577, https://doi.org/10.1021/acs.est.1c07121, 2022.

Syafira, S. A., Effendi, M. D., and Romadhon, M. S. (2026**).** Comparative review of laboratory approaches for simulating and characterizing aerosol emissions from open biomass burning. *Environmental Science: Atmospheres, 6*, 786–809. https://doi.org/10.1039/D5EA00146C

Syafira, S. A., Hu, D., Voliotis, A., Wu, H., Oghama, O. E., Shao, Y., Budisulistiorini, S. H., Wang, Y., Flynn, M., Gallimore, P. J., Coe, H., Allan, J., and McFiggans, G.: Method-Dependent Variability in Hygroscopicity Parameter (κ) of Particles from Biomass-Burning Across Fuel Types and Burn Phases, EGUsphere [preprint], https://doi.org/10.5194/egusphere-2026-2723, 2026.

Tang, R., et al.: Biomass-burning-induced surface darkening and its impact on regional meteorology in China, Atmos. Chem. Phys., 20, 6177–6191, https://doi.org/10.5194/acp-20-6177-2020, 2020.

Tian, J., et al.: A biomass combustion chamber: design and wheat straw combustion case study, Aerosol Air Qual. Res., 15, 2104–2114, https://doi.org/10.4209/aaqr.2015.03.0167, 2015.

Tiitta, P., et al.: Transformation of logwood combustion emissions: SOA formation with aging, Atmos. Chem. Phys., 16, 13251–13269, https://doi.org/10.5194/acp-16-13251-2016, 2016.

Voliotis, A., et al.: Composition and volatility of SOA in mixed precursor systems, Atmos. Chem. Phys., 21, 14251–14273, https://doi.org/10.5194/acp-21-14251-2021, 2021.

Wang, J., et al.: Evolution of water uptake of SOA in chamber experiments, Atmos. Chem. Phys., 22, 4149–4166, https://doi.org/10.5194/acp-22-4149-2022, 2022.

Yao, L., et al.: Emissions of toxic substances from biomass burning: a review, Processes, 11, 853, https://doi.org/10.3390/pr11030853, 2023.

Ye, Q., et al.: Oxygenated organic compounds in gas and particle phases via iodide CIMS, Atmos. Chem. Phys., 21, 8455–8478, https://doi.org/10.5194/acp-21-8455-2021, 2021.

Zhai, J., Lu, X., Li, L., Zhang, Q., Zhang, C., Chen, H., Yang, X., and Chen, J.: Size-resolved chemical composition, effective density, and optical properties of biomass burning particles, Atmos. Chem. Phys., 17, 7481–7493, https://doi.org/10.5194/acp-17-7481-2017, 2017.

Zhong, Q., et al.: Attributing modelled aerosol biases in biomass burning regions using satellite observations, Nat. Commun., 13, 5914, https://doi.org/10.1038/s41467-022-33680-4, 2022.

https://doi.org/10.5194/egusphere-2026-4932
Preprint. Discussion started: 10 September 2026

689 Zhuravleva, T. B., et al.: Photochemical evolution of BB aerosol and radiative forcing efficiency: a box model, Atmosphere, 12,
690 1555, https://doi.org/10.3390/atmos12121555, 2021.